ChemComm

COMMUNICATION

First-order hyperpolarizabilities of chiral, polymer-wrapped single-walled carbon nanotubes†

Cite this: *Chem. Commun.*, 2016, 52, 12206

Received 28th July 2016,
Accepted 7th September 2016

DOI: 10.1039/c6cc06190g

www.rsc.org/chemcomm

Griet Depotter,[a] Jean-Hubert Olivier,[b] Mary G. Glesner,[b] Pravas Deria,‡[b] Yusong Bai,[b] George Bullard,[b] Amar S. Kumbhar,[c] Michael J. Therien*[b] and Koen Clays*[a]

We report the first-order hyperpolarizabilities (β_{HRS} values) of individualized, length-sorted (700 ± 50 nm long) (6,5) SWNTs and corresponding polymer-wrapped (6,5) SWNT superstructures. These SWNT-based nanohybrids feature semiconducting polymers that wrap the SWNT surface in an exclusive left-handed helical fashion. Manipulation of the polymer electronic structures in these well-defined nanoscale objects provides a new avenue to modulate the magnitude of β_{HRS} at long wavelength (1280 nm).

The unique optical[1,2] and electrical properties[3] of semiconducting single-walled carbon nanotubes (SWNTs) fuel the development of SWNT-based nanohybrid materials for opto-electronic, and photonic applications.[4] The near infrared (NIR) electronic absorptive spectral signatures of SWNTs suggest these nanoscale structures as components of non-linear optical (NLO) materials relevant to the telecommunication spectral window (1000–2000 nm). While SWNT linear optical properties are well characterized, only a handful of studies have examined the NLO responses of SWNT-based materials.[5–8] Challenges faced in characterizing carbon nanotube NLO response include: (i) probing SWNT samples that feature homogeneous composition; (ii) organizing SWNTs into hierarchical mesoscale materials that preserve electro-optic properties manifest at the single-tube level; and (iii) developing non-destructive SWNT functionalization strategies that exploit pristine nanotubes and hyperpolarizable chromophores and give rise to new materials having enhanced NLO properties.

In contrast to covalent sidewall functionalization that disrupts the delocalized nanotube electronic structure, molecular surfactants exfoliate and individualize semiconducting SWNTs. Non-covalent surfactant functionalization of SWNTs, however, suffers from the inabilities to: (i) control the stoichiometry of molecular NLO dipoles or octopoles at the nanotube interface, (ii) structure electro-optically functional SWNT-based nanohybrids over macroscopic length scales, and (iii) engineer nanotube-soft matter assemblies in which NLO properties can be rigorously elucidated and ultimately modulated. This latter challenge is of critical importance, as optimization of first- and second-order hyperpolarizabilities requires fundamental new insights into the design of hybrid nanomaterial electronic structures.

Here we report for the first time the second order NLO responses of SWNT-based nanohybrid compositions based on (6,5) chirality enriched, length-sorted (700 ± 50 nm long) SWNTs ([(6,5) SWNTs]), and chiral polymers that have previously been established to wrap SWNTs in an exclusive left-handed helical fashion (see ESI†).[9] All of these polymer–SWNT superstructures have been structurally characterized.[9–12] The semiconducting polymers ***S*-PBN(b)–Ph_2PZn_2** and ***S*-PBN(b)–Ph_2PZn_3** feature respectively dimeric and trimeric *meso*-to-*meso* ethyne-bridged (porphinato)zinc(II) units integrated into the conjugated polymer backbone,[13] while the ***S*-PBN(b)–PZnRuPZn** polymer exploits a **PZnRuPZn** supermolecular chromophore in the polymer repeat unit where (porphinato)zinc(II) (PZn) and ruthenium(II)polypyridyl (Ru) structures are connected *via* a macrocycle *meso*-to-4′-terpyridyl ethyne bridge.[14,15] It is important to note that **PZn_2**, **PZn_3**, and **PZnRuPZn** monomers have been established as potent octopolar NLO chromophores.[14,15] Depictions of the polymer–SWNT superstructures based on these established NLO-active chromophores, ***S*-PBN(b)–Ph_2PZn_2–[(6,5) SWNT]**, ***S*-PBN(b)–Ph_2PZn_3–[(6,5) SWNT]**, and ***S*-PBN(b)–PZnRuPZn–[(6,5) SWNT]**, along with that for a benchmark superstructure, **PNES–[(6,5) SWNT]**, are shown in Scheme 1.

These chiral polymers are members of a class of highly charged [arylene]ethynylene polymers that have previously been established to exfoliate, individualize, and single-chain wrap the nanotube surface with periodic and constant morphology.[9–12,16,17] Extensive AFM and TEM data demonstrate a helix pitch length

[a] *Department of Chemistry, University of Leuven, Celestijnenlaan 200D, B-3001 Leuven, Belgium*
[b] *Department of Chemistry, French Family Science Center, Duke University, 124 Science Drive, Durham, North Carolina 27708, USA. E-mail: michael.therien@duke.edu; Fax: +1 919 684 1522; Tel: +1 919 660 1670*
[c] *Chapel Hill Analytical & Nanofabrication Laboratory, University of North Carolina at Chapel Hill, 243 Chapman Hall, Chapel Hill, North Carolina 27559, USA. E-mail: koen.clays@fys.kuleuven.be; Fax: +32 1 632 7982; Tel: +32 1 632 7508*

† Electronic supplementary information (ESI) available: Synthetic, spectroscopic, and characterization details. See DOI: 10.1039/c6cc06190g

‡ Present address: Department of Chemistry & Biochemistry, Southern Illinois University-Carbondale, Carbondale, Illinois 62901, USA.

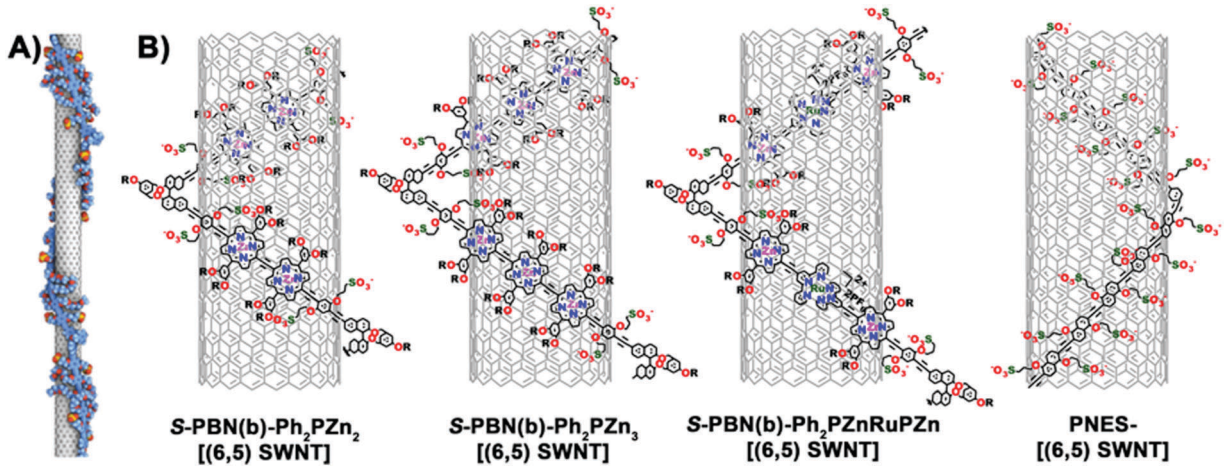

Scheme 1 (A) Depiction of a chiral [arylene]ethynylene polymer-wrapped SWNT. (B) Schematic representations of NLO active superstructures ***S*-PBN(b)–Ph_2PZn_2–[(6,5) SWNT]**, ***S*-PBN(b)–Ph_2PZn_3–[(6,5) SWNT]**, ***S*-PBN(b)–$Ph_2PZnRuPZn$–[(6,5) SWNT]**, and the control superstructure **PNES-[(6,5) SWNT]**.

of 9 ± 2 nm for the nanohybrid polymer-wrapped ***S*-PBN(b)–Ph_2Zn_2–[(6,5) SWNT]** and ***S*-PBN(b)–PZnRuPZn–[(6,5) SWNT]** super-structures, and 6 ± 2 nm for the ***S*-PBN(b)–Ph_2Zn_3–[(6,5) SWNT]** assembly (Fig. S7–S10, ESI†). It is important to note that (i) these semiconducting polymer–SWNT superstructures are robust in a wide range of aqueous and organic solvents,[9–11,16] and (ii) this single chain polymer-wrapping mechanism solubilizes the nanotube at a minimal polymer : SWNT molar ratio, and provides a facile means to organize functional organic moieties at predefined intervals along the SWNT surface.[12] As the NLO properties of the **PZn_2**, **PZn_3**, and **PZnRuPZn** units arise from conformeric populations having D_2 and D_{2d} symmetries at ambient temperature in solution,[15] probing the first-order hyperpolarizability of these polymer-wrapped (6,5) SWNT nanohybrids *via* the hyper-Rayleigh light scattering (HRS) technique provides insight into emergent NLO properties of chirality enriched (6,5) SWNTs, and opportunities to investigate the magnitude to which the SWNT scaffold impacts the β value that characterizes conformationally restricted chromophores.

Linear optical properties. Fig. 1 and Fig. S13 (ESI†) chronicle ground-state electronic absorption (EA) spectra of polymer-wrapped (6,5) SWNT nanohybrids and a sodium cholate surfactant-dispersed (6,5) SWNT (**SC–[(6,5) SWNT]**) sample; Table S1 (ESI†) summarizes key optical transitions and associated full widths at half maximum (FWHM) that characterize the unbound polymers and corresponding superstructures. Poly[2,6-1,5-bis(3-propoxysulfonicacid sodiumsalt)-naphthylene]ethynylene (PNES)[11] has been utilized to engineer a control superstructure, **PNES–[(6,5) SWNT]**,[11] in which the highly charged semiconducting polymer acts solely as a (6,5) SWNT exfoliating agent. Modest bathochromic shifts of the (6,5) SWNT E_{11} and E_{22} transitions (22 meV and 26 meV, respectively) for **PNES–[(6,5) SWNTs]** are observed relative to those characteristic of **SC–[(6,5) SWNTs]** in aqueous solvent: previous work suggests that such modest SWNT E_{nn} spectral shifts derive in large part from differences in the extent to which polymer-wrapped nanotube samples are solvated relative to SC surfactant-dispersed SWNTs.[18]

Fig. S13A and B (ESI†) display vis-NIR absorption data pertinent to the ***S*-PBN(b)–Ph_2Zn_2–[(6,5) SWNT]** superstructure

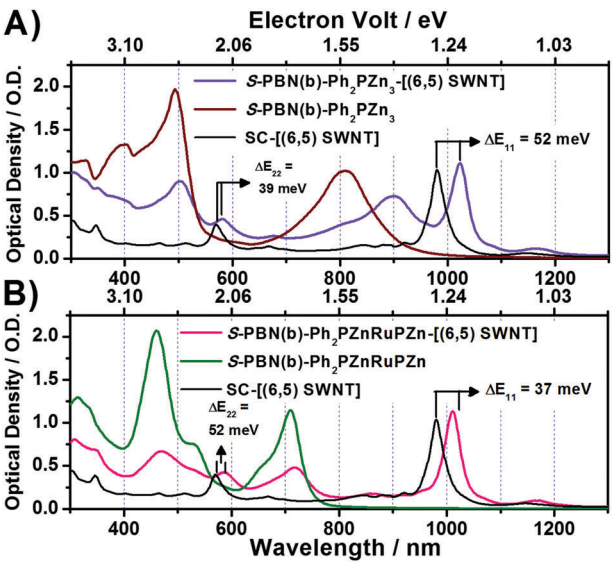

Fig. 1 Electronic absorption spectra of: (A) ***S*-PBN(b)–Ph_2Zn_3–[(6,5) SWNTs]** (violet) and the unbound ***S*-PBN(b)–Ph_2Zn_3** polymer (burgundy) recorded in 4 : 6 CH_3CN/D_2O solvent; [(6,5) SWNT] = 101.7 nM. (B) ***S*-PBN(b)–$Ph_2PZnRuPZn$–[(6,5) SWNTs]** (pink) and the unbound ***S*-PBN(b)–PZnRuPZn** polymer (green) recorded in 4 : 6 CH_3CN/D_2O solvent; [(6,5) SWNT] = 103.1 nM. Note that in each panel, the spectrum of surfactant-dispersed **SC–[(6,5) SWNTs]** (black) is shown at [(6,5) SWNT] = 94.0 nM.

and its component ***S*-PBN(b)–Ph_2Zn_2** polymer. The EA spectrum of the chiral ***S*-PBN(b)–Ph_2Zn_3** polymer presented in Fig. 1A manifests features reminiscent of the parent *meso*-to-*meso* ethyne-bridged **PZn_3** oligomer: (i) strong and complex absorptive bands that span the UV-vis region (345–550 nm) with two peak maxima at 399 and 490 nm assigned to B_y- and B_x-derived π–π* transitions, and (ii) a low-energy Q-state derived π–π* transition manifold centered at 808 nm (FWHM = 0.245 eV) that is polarized exclusively along the long molecular axis.[13] Similar to the ***S*-PBN(b)–Ph_2Zn_2–[(6,5) SWNT]** superstructure, ***S*-PBN(b)–Ph_2Zn_3–[(6,5) SWNTs]** evince substantial $E_{00} \rightarrow E_{11}$ and $E_{00} \rightarrow E_{22}$ spectral red shifts relative to the **SC–[(6,5) SWNT]** composition (39 and 52 meV, respectively; Fig. 1A). The **PZn_3**

Q_x-derived transition manifold maximum in ***S*-PBN(b)–Ph_2Zn_3–[(6,5) SWNTs]** (λ_{max} = 901 nm) significantly red shifts relative to that of unbound ***S*-PBN(b)–Ph_2Zn_3** polymer (λ_{max} = 808 nm). The spectral breadth of the **PZn_3** Q_x-derived transition manifold of the ***S*-PBN(b)–Ph_2Zn_3–[(6,5) SWNT]** superstructure (FWHM = 0.180 eV) narrows considerably relative to that determined for the unbound ***S*-PBN(b)–Ph_2Zn_3** polymer (FWHM = 0.245 eV), congruent with both a more limited range of accessible **PZn_3** conformers and a dramatically reduced mean torsional angle between adjacent (porphinato)zinc units when the polymer wraps the nanotube sidewall.

The chiral polymer ***S*-PBN(b)–Ph_2PZnRuPZn** exploits a chromophoric motif in which (porphinato)zinc(II) and ruthenium(II)polypyridyl (Ru) units are connected *via* an ethyne bridge. In PZnMPZn supermolecules, PZn π–π* and metal polypyridyl-based charge-resonance absorption oscillator strength are extensively mixed, and the respective charge transfer transition dipoles of these building blocks are aligned along the highly conjugated molecular axis.[14,15,19,20] The non-dipolar **PZnRuPZn** building block defines an exceptional class of octopolar NLO chromophores: HRS depolarization experiments show that the measured hyperpolarizability (β_{HRS} values) of these structures arises predominantly from conformers with torsional angles between the terpyridyl units and the PZn plane that are approximately equal in magnitude and opposite in sign, suggesting that modest solution-phase D_2 or D_{2d} structural subpopulations of these PZnMPZn chromophores possess exceptional hyperpolarizabilities.[15] EA spectra of the parent ***S*-PBN(b)–Ph_2PZnRuPZn** polymer and the ***S*-PBN(b)–Ph_2PZnRuPZn–[(6,5) SWNT]** superstructure are shown in Fig. 1B. The unbound ***S*-PBN(b)–Ph_2PZnRuPZn** polymer evinces spectroscopic signatures associated to **PZnRuPZn** derivatives: (i) a UV absorption at 311 nm that reflects substantial terpyridine-localized $^1\pi$–π* character, (ii) a strong (ε = 205 000 M^{-1} cm^{-1}) absorption manifold centered at 460 nm which exhibits significant porphyrin-derived $^1\pi$–π* Soret (B) band character, (iii) a visible band centered at 529 nm which exhibits $[Ru(tpy)_2]^{2+}$-derived singlet metal-to-ligand charge transfer (^{1}MLCT) character and features contributions from porphyrin ligand oscillator strength, and (iv) an EA manifold having a maximum at 710 nm (ε = 109 000 M^{-1} cm^{-1}) which exhibits substantial porphyrinic $^1\pi$–π* Q-state character and augmented oscillator strength that derives from charge resonance contributions driven by the ethyne-bridged porphyrin *meso*-carbon-to-terpyridyl-4-carbon linkage.[14,19–21]

The apparent red shift of the (6,5) SWNT $E_{00} \rightarrow E_{11}$ transition in ***S*-PBN(b)–Ph_2PZnRuPZn–[(6,5) SWNTs]** (E_{11} = 1011 nm, ΔE_{11} = 38 meV) relative to the benchmark **SC–[(6,5) SWNT]** composition (E_{11} = 980 nm) is less pronounced than that observed for ***S*-PBN(b)–Ph_2Zn_3–[(6,5) SWNTs]** (ΔE_{11} = 52 meV), and suggests a weaker electronic interaction of the chiral polymer chain with the nanotube. Equally notable are the modest bathochromic shift (19 meV) of the Q_x-derived absorption manifold maximum observed for the ***S*-PBN(b)–Ph_2PZnRuPZn–[(6,5) SWNT]** superstructure (λ_{max} = 718 nm; FWHM = 0.154 eV) compared to that recorded for unbound ***S*-PBN(b)–Ph_2PZnRuPZn** polymer (λ_{max} = 710 nm; FWHM = 0.154 eV), and the fact that the superstructure's Q_x-derived spectral band shape is essentially unperturbed relative to that for the free polymer; these data thus suggest that in contrast to the ***S*-PBN(b)–Ph_2PZn_2** and ***S*-PBN(b)–Ph_2PZn_3** polymers, helical wrapping of the ***S*-PBN(b)–Ph_2PZnRuPZn** polymer on the (6,5) SWNT surface does not significantly impact the conformeric distribution of its constituent **PZnRuPZn** chromophores.

Non-linear optical properties of polymer-wrapped [(6,5) SWNTs]. With individualized, non-covalent functionalized **PNES–[(6,5) SWNTs]** and **SC–[(6,5) SWNTs]**, the experimentally observed hyper-Rayleigh light intensity originating from these well-defined individual scattering centers may be related to a single nanotube β_{HRS} value. The second-order nonlinear nature of this optical response traces its origin to: (i) the energies of the E_{11} transitions, (ii) the intrinsic chirality of these SWNTs, and (iii) for the polymer-wrapped SWNT samples, the helically chiral nature of the superstructure.[9] For the **SC–[(6,5) SWNT]** and **PNES–[(6,5) SWNT]** benchmarks, these individual nanotube hyperpolarizability (β_{HRS}) values correspond respectively to 1050 ± 140 and 1220 ± 160 × 10^{-30} esu (Table 1); note that these values are in excellent agreement with the bulk susceptibility value, $\chi^{(2)}_{xyz}$, of ~10^{-6} esu calculated within DFT in the local-density approximation (ESI†).[22]

Table 1 data demonstrate that it is possible to further enhance the individual SWNT second-order NLO response by exploiting highly charged semiconducting [arylene]ethynylene polymers that provide single-handed SWNT helical wrapping. For the ***S*-PBN(b)–Ph_2PZn_2–[(6,5) SWNT]**, ***S*-PBN(b)–Ph_2PZn_3–[(6,5) SWNT]**, and ***S*-PBN(b)–Ph_2PZnRuPZn–[(6,5) SWNT]** superstructures, the detailed nature of the β_{HRS} enhancements derives from an intricate interplay between modulation of the electronic properties of the nanotube by the semiconducting polymer that wraps its surface, and the modulation of

Table 1 β_{HRS} values for ***S*-PBN(b)–Ph_2PZn_2–[(6,5) SWNT]**, ***S*-PBN(b)–Ph_2PZn_3–[(6,5) SWNT]**, and ***S*-PBN(b)–Ph_2PZnRuPZn–[(6,5) SWNT]** superstructures, benchmark **SC–[(6,5) SWNT]** and **PNES–[(6,5) SWNT]** samples, and those determined for their respective constituents. Note that β_{SWNT} is the measured hyperpolarizability of the individualized (6,5) SWNT, β_{chromo} the value of the chromophoric building block, β_{mono} the hyperpolarizability of the monomer determined in the free polymer, and $\beta_{mono,wrap}$ is the calculated hyperpolarizability of the monomers determined from measurements of polymer–SWNT superstructures (see ESI for detailed description of these measurements and calculations)

Opto-electronic material	β_{SWNT}[a]	β_{chromo}	β_{mono}[a]	$\beta_{mono,wrap}$[a]
SC–[(6,5) SWNT]	1050 ± 140			
PNES–[(6,5) SWNT]	1220 ± 160		10 ± 2	8 ± 2
***S*-PBN(b)–Ph_2PZn_2–[(6,5) SWNT]**	2040 ± 270	410 ± 60[b] [15]	150 ± 20	95 ± 20
***S*-PBN(b)–Ph_2PZn_3–[(6,5) SWNT]**	1480 ± 190	580 ± 50[b]	130 ± 20	55 ± 20
***S*-PBN(b)–PZnRuPZn–[(6,5) SWNT]**	1720 ± 210	800 ± 30[b] [23]	150 ± 20	95 ± 20

[a] $\beta_{HRS,1280}$ in units of 10^{-30} esu, irradiation wavelength = 1280 nm. [b] $\beta_{HRS,1300}$ in units of 10^{-30} esu, irradiation wavelength = 1300 nm.

chromophore conformation that results from the tight polymer wrapping around the SWNT.

A rigorous interpretation of the HRS intensity determined for these polymer-wrapped SWNT superstructures is thus complicated by the fact that in these chiral assemblies, the electronic properties of both the polymer and the nanotube are modulated relative to that of the free polymer and an **SC–[(6,5) SWNT]**. While it is possible to measure β_{HRS} of the component elements of these structures [*i.e.*, the **SC–[(6,5) SWNT]** benchmark, **PZn_2**, **PZn_3**, and **PZnRuPZn** chromophores (βchromo, Table 1), and that for the polymer repeat unit (β_{mono}, Table 1)], such values cannot be considered as invariant characteristics of the components due to the electronic interplay between SWNT and polymer; such an analysis is further complicated by the fact that it is not possible to make conclusions regarding specific phase relations of the polymer- and SWNT-derived signals that contribute to the measured NLO response.

Within the scope of these considerations, certain qualitative conclusions may be made regarding the factors that contribute to the NLO responses determined for the ***S*-PBN(b)–Ph_2PZn_2–[(6,5) SWNT]**, ***S*-PBN(b)–Ph_2PZn_3–[(6,5) SWNT]**, and ***S*-PBN(b)–Ph_2PZnRuPZn–[(6,5) SWNT]** superstructures. If the principle contributors to the enhanced hyperpolarizabilities in these constructs derive from the modest extent to which the (6,5) SWNT is electronically perturbed relative to the **SC–[(6,5) SWNT]** benchmark (β_{HRS} = 1050 × 10^{-30} esu), and the degree to which polymer wrapping modulates the NLO response of the chromophore component of the polymer repeat unit, these superstructures may be approximated as two-component systems,[24] and an estimate $\beta_{mono,wrap}$ (Table 1), the monomeric chromophore hyperpolarizability when wrapped around the SWNT, may be obtained. Note that in these superstructures, the lowest-energy absorption maximum (Table S1, ESI†) red shifts relative to the analogous absorption of their respective polymeric components. Given the HRS 1280 nm fundamental irradiation wavelength, each of the low energy transition manifolds in these superstructures shifts away from the 640 nm second-harmonic wavelength: the degree of two-photon resonance enhancement hence decreases for each superstructure relative to that for the component polymer. As this red shift correlates with the extent of chromophore unit planarization, SWNT polymer wrapping likely renders these D_2-symmetric chromophores more centrosymmetric, and, hence, less chiral and less second-order NLO active.[15]

In summary, we report for the first time experimental measurements of the first-order hyperpolarizability of individualized, length-sorted (700 ± 50 nm long) single chirality (6,5) SWNTs. We determine a β_{HRS} (1050 × 10^{-30} esu) value for surfactant-encapsulated **SC–[(6,5) SWNTs]**, and show that in single-chain, semiconducting polymer-wrapped [(6,5) SWNT] superstructures, manipulation of polymer electronic structure provides a new avenue to modulate the magnitude of β_{HRS} at a telecommunication-relevant wavelength (1280 nm). These (6,5) SWNT-based nanohybrids, based on chiral, opto-electronically active [arylene]ethynylene polymers that helically wrap the nanotube surface in an exclusive left-handed, single-chain helical fashion, feature **PZn_2**, **PZn_3** and **PZnRuPZn** octopolar chromophores as integral parts of the polymer backbone. While the polymer–nanotube electronic interaction for these chiral superstructures diminishes the magnitude of 2-photon resonance enhancement of β_{HRS} for a 1280 nm fundamental irradiation wavelength, the combination of polymer-modulated $E_{00} \rightarrow E_{nn}$ transition red-shifts, the use of nanotube chiralities having intrinsically smaller bandgaps, and polymer electronic structural modification, offer opportunities to engineer electro-optically active nanoscale superstructures that feature enhanced hyperpolarizabilities over the 1.5–2 μm spectral domain.

This work was supported by the Division of Chemical Sciences, Geosciences, and Biosciences, Office of Basic Energy Sciences, of the U.S. Department of Energy through Grant DE-SC0001517, the Fund for Scientific Research-Flanders (Research Grant No. 1510712N), and the University of Leuven (GOA/2011/03).

Notes and references

1 L. J. Carlson and T. D. Krauss, *Acc. Chem. Res.*, 2008, **41**, 235–243.
2 P. Avouris, M. Freitag and V. Perebeinos, *Nat. Photonics*, 2008, **2**, 341–350.
3 P. Avouris, Z. Chen and V. Perebeinos, *Nat. Nanotechnol.*, 2007, **2**, 605–615.
4 M. S. Arnold, J. L. Blackburn, J. J. Crochet, S. K. Doorn, J. G. Duque, A. Mohite and H. Telg, *Phys. Chem. Chem. Phys.*, 2013, **15**, 14896–14918.
5 J. Wang, Y. Chen and W. J. Blau, *J. Mater. Chem.*, 2009, **19**, 7425–7443.
6 J. Wang, K.-S. Liao, D. Früchtl, Y. Tian, A. Gilchrist, N. J. Alley, E. Andreoli, B. Aitchison, A. G. Nasibulin, H. J. Byrne, E. I. Kauppinen, L. Zhang, W. J. Blau and S. A. Curran, *Mater. Chem. Phys.*, 2012, **133**, 992–997.
7 W. Zhao, *J. Phys. Chem. Lett.*, 2011, **2**, 482–487.
8 S. Cambré, J. Campo, C. Beirnaert, C. Verlackt, P. Cool and W. Wenseleers, *Nat. Nanotechnol.*, 2015, **10**, 248–252.
9 P. Deria, C. D. Von Bargen, J.-H. Olivier, A. S. Kumbhar, J. G. Saven and M. J. Therien, *J. Am. Chem. Soc.*, 2013, **135**, 16220–16234.
10 Y. K. Kang, O.-S. Lee, P. Deria, S. H. Kim, T.-H. Park, D. A. Bonnell, J. G. Saven and M. J. Therien, *Nano Lett.*, 2009, **9**, 1414–1418.
11 P. Deria, L. E. Sinks, T.-H. Park, D. M. Tomezsko, M. J. Brukman, D. A. Bonnell and M. J. Therien, *Nano Lett.*, 2010, **10**, 4192–4199.
12 J.-H. Olivier, J. Park, P. Deria, J. Rawson, Y. Bai, A. S. Kumbhar and M. J. Therien, *Angew. Chem., Int. Ed.*, 2015, **54**, 8133–8138.
13 V. S.-Y. Lin, S. G. DiMagno and M. J. Therien, *Science*, 1994, **264**, 1105–1111.
14 H. T. Uyeda, Y. Zhao, K. Wostyn, I. Asselberghs, K. Clays, A. Persoons and M. J. Therien, *J. Am. Chem. Soc.*, 2002, **124**, 13806–13813.
15 T. V. Duncan, K. Song, S.-T. Hung, I. Miloradovic, A. Nayak, A. Persoons, T. Verbiest, M. J. Therien and K. Clays, *Angew. Chem., Int. Ed.*, 2008, **47**, 2978–2981.
16 J.-H. Olivier, P. Deria, J. Park, A. Kumbhar, M. Andrian-Albescu and M. J. Therien, *Angew. Chem., Int. Ed.*, 2013, **52**, 13080–13085.
17 C. D. Von Bargen, C. M. MacDermaid, O.-S. Lee, P. Deria, M. J. Therien and J. G. Saven, *J. Phys. Chem. B*, 2013, **117**, 12953–12965.
18 B. A. Larsen, P. Deria, J. M. Holt, I. N. Stanton, M. J. Heben, M. J. Therien and J. L. Blackburn, *J. Am. Chem. Soc.*, 2012, **134**, 12485–12491.
19 T. Ishizuka, L. E. Sinks, K. Song, S.-T. Hung, A. Nayak, K. Clays and M. J. Therien, *J. Am. Chem. Soc.*, 2011, **133**, 2884–2896.
20 T. V. Duncan, T. Ishizuka and M. J. Therien, *J. Am. Chem. Soc.*, 2007, **129**, 9691–9703.
21 X. Hu, D. Xiao, S. Keinan, I. Asselberghs, M. J. Therien, K. Clays, W. Yang and D. N. Beratan, *J. Phys. Chem. C*, 2010, **114**, 2349–2359.
22 G. Y. Guo, K. C. Chu, D.-s. Wang and C.-g. Duan, *Phys. Rev. B: Condens. Matter Mater. Phys.*, 2004, **69**, 205416.
23 A. Nayak, PhD thesis, University of Pennsylvania, 2011.
24 K. Clays and A. Persoons, *Phys. Rev. Lett.*, 1991, **66**, 2980–2983.